Electronic Supplementary Material (ESI) for ChemComm.

Supporting Information for:

Temperature Insensitive Fluorescence Intensity in a Coumarin Monomer-Aggregate Coupled System

Xiaogang Liu,[a†] Deqi Mao,[b,c†] Jacqueline M. Cole,[a,d*] and Zhaochao Xu[b,c*]

[a]Cavendish Laboratory, Department of Physics, University of Cambridge, J. J. Thomson Avenue, Cambridge, CB3 0HE, UK.

[b]Key Laboratory of Separation Science for Analytical Chemistry, Dalian Institute of Chemical Physics, Chinese Academy of Sciences, 457 Zhongshan Road, Dalian 116023, China, +86-411-84379648.

[c]State Key Laboratory of Fine Chemicals, Dalian University of Technology, 2 Linggong Road, Dalian 116012, China.

[d]Argonne National Laboratory, 9700 S Cass Avenue, Argonne, IL 60439, USA.

[†]These authors contributed equally.

Contents

List of Figures

List of Tables

Materials and Instruments

All reagents were purchased from commercial suppliers and used without further purification, unless stated otherwise.

^{1}H-NMR and ^{13}C-NMR spectra were recorded on a VARIAN INOVA-400 spectrometer, using TMS as an internal standard. Mass spectrometry data were obtained with a HP1100LC/MSD mass spectrometer and a LC/Q-TOF MS spectrometer. UV-Vis absorption spectra were collected on a Cary 60 UV-Vis spectrophotometer. Fluorescence measurements were performed on an Agilent CARY Eclipse fluorescence spectrophotometer with Single Cell Peltier temperature controller. For measurements of fluorescence decay dynamics, a pulsed diode laser of 405 nm was used as the excitation source. The emission of **1** was measured using time-correlated single photon counting (TCSPC) setup from Edinburgh Instruments (OB 920).

Chemical Synthesis and Characterization

Scheme S1: synthesis of 7-dimethylaminocoumarin-3-aldehyde (**1**)

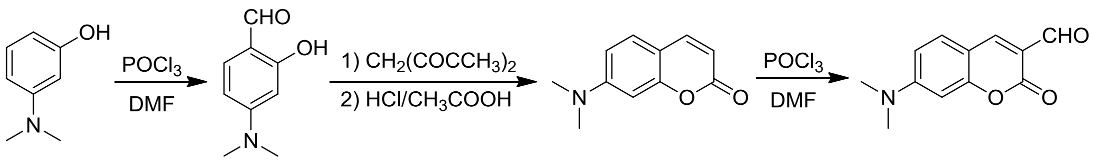

2 **3** **4** **1**

Synthesis of 4-(dimethylamino)-2-hydroxybenzaldehyde (3)

POCl$_3$ (2.0 mL, 1.5 eqv.) was added slowly to dry DMF at 0 °C and stirred for 30 min. 3-(Dimethylamino)-phenol (2.00 g, 14.6 mmol) dissolved in dry DMF was then slowly added to the reaction mixture at 0 °C. The solution was warmed to 80 °C and stirred overnight. The reaction mixture was poured into ice and stirred for several minutes. The resulting solution, containing precipitate, was adjusted to neutral pH using 4 M sodium hydroxide solution. The solid was filtered and purified via column chromatography by eluting with ethyl acetate/n-hexane (EA:hexane = 1:3, v/v) to yield the product as a yellow solid (916 mg, yield: 38%). ^{1}H NMR (400 MHz , CDCl$_3$) δ 11.59 (s, 1H), 9.52 (s, 1H), 7.28 (d, *J* = 8.9 Hz, 1H), 6.28 (dd, *J* = 8.8Hz, 2.4 Hz , 1H), 6.07 (s, 1H), 3.06 (s, 6H). HRMS (ESI) calcd for $C_9H_{12}NO_2$ $[M+H]^+$ 166.0868, found 166.0870.

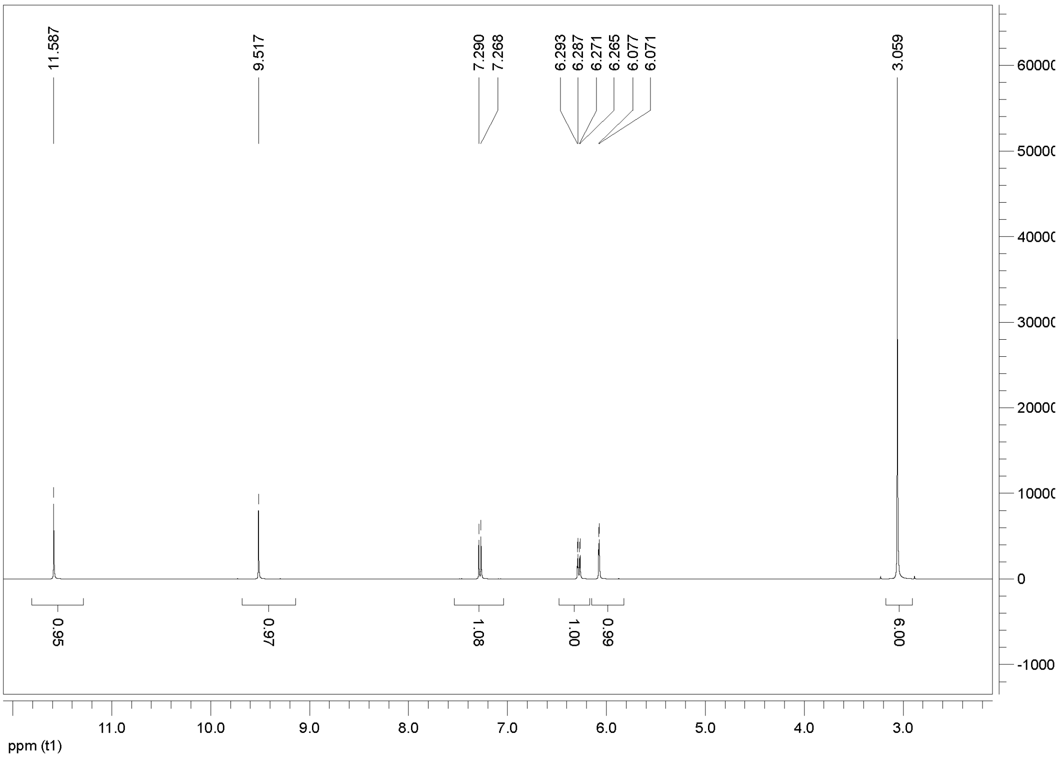

Figure S1: ^{1}H-NMR of **3** in $CDCl_3$.

Synthesis of 7-dimethylaminocoumarin (4)

4-Dimethylaminosalicylaldehyde (250 mg, 1.51 mmol), dimethylmalonate (400 mg, 3.02 mmol) and piperidine (0.5 mL) were mixed in absolute ethanol (10 mL) and stirred for 6 hours under reflux conditions. Ethanol was evaporated under reduced pressure. After that, concentrated HCl (10 mL) and glacial acetic acid (10 mL) were added to hydrolyze the reaction with stirring for another 6 hours. The solution was cooled to room temperature and poured into 100 mL ice water. NaOH solution (40%) was added dropwise to modulate pH of the solution to ~5, and a pale precipitate formed immediately. After stirring for 30 mins, the mixture was filtered, washed with water, dried, and then recrystallized with toluene to give **4** (200 mg, yield: 70%) .^{1}H-NMR (400 M Hz, $CDCl_3$) δ 7.55 (d, *J* = 9.2 Hz, 1H), 7.26 (d, *J* = 8.8 Hz, 1H), 6.60 (dd, *J* = 8.8, 2.4Hz, 1H,), 6.51 (s, 1H), 6.06 (d, *J* = 9.6 Hz, 1H), 3.05 (s, 6H); ^{13}C-NMR (CD_3Cl, 100 MHz) δ 162.10, 156.38, 152.97, 143.67, 128.51, 109.90, 109.02, 108.81, 98.18, 40.15; HRMS (ESI) calcd for $C_{11}H_{12}NO_2$ $[M+H]^+$ 190.0868, found 190.0872.

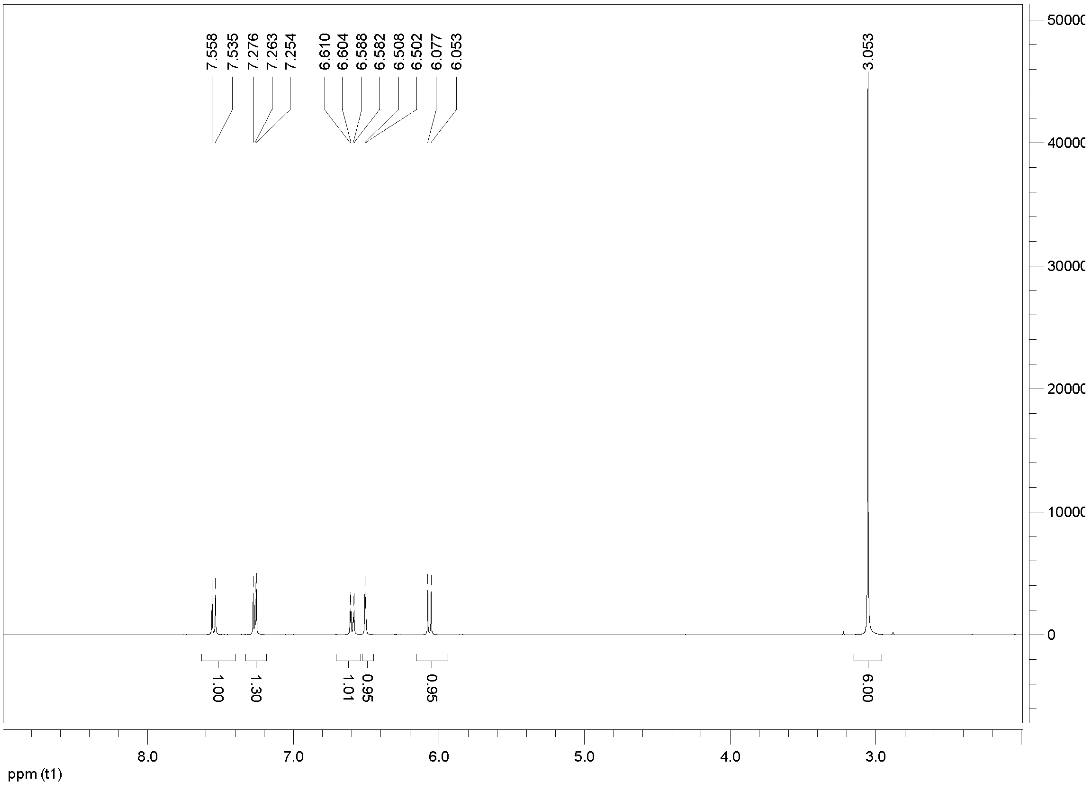

Figure S2: ^{1}H-NMR spectrum of **4** in CDCl$_3$.

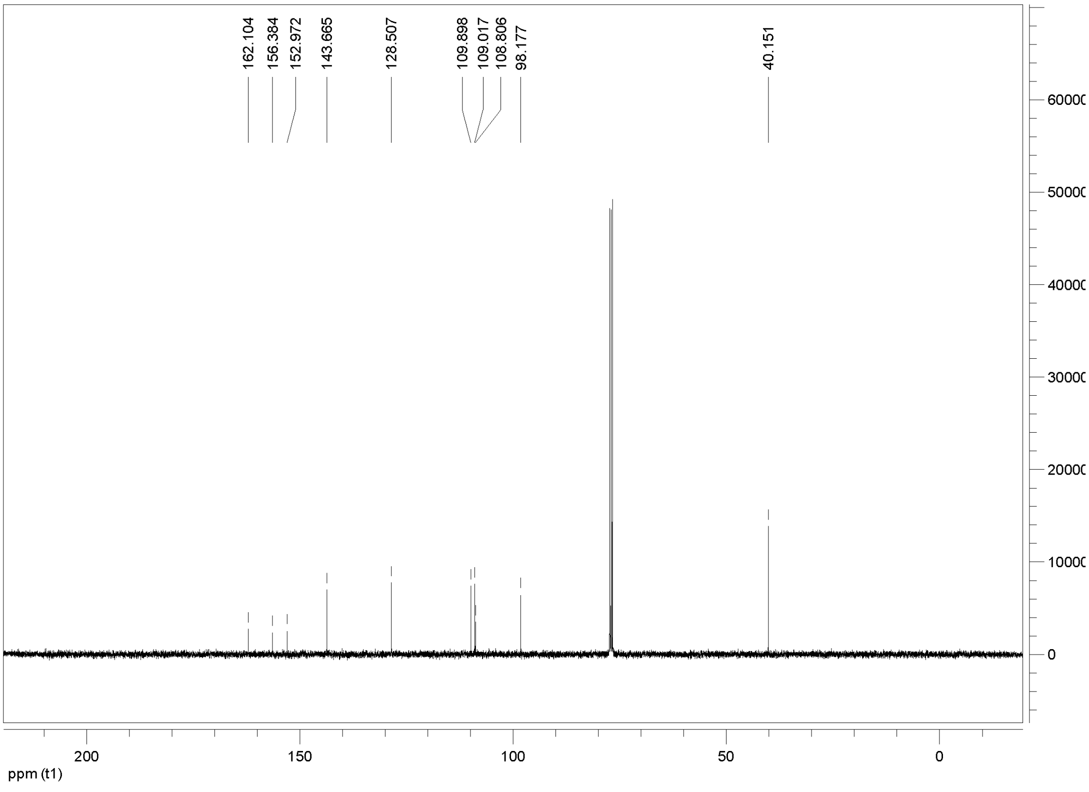

Figure S3: ^{13}C-NMR spectrum of **4** in CDCl$_3$.

Synthesis of 7-dimethylaminocoumarin-3-aldehyde (1)

Fresh distilled DMF (2 mL) was added dropwise to $POCl_3$ (0.3 mL) at 20-50 °C in N_2 atmosphere and stirred for 30 minutes to yield a red solution. This solution was combined with a portion of **4** (200 mg, 1.06 mmol, dissolved in 3 mL DMF) to afford a scarlet colored suspension. The mixture was stirred at 60 °C for 12 hours and then poured into 100 mL of ice water. NaOH solution (20%) was added to adjust pH of the mixture to yield large amount of precipitate. The crude product was filtered, thoroughly washed with water, dried and recrystallized in absolute ethanol to give **1** (126 mg, yield: 55%). ^{1}H-NMR (400M Hz, $CDCl_3$) δ 10.14 (s, 1H), 8.26 (s, 1H), 7.43 (d, J = 8.8 Hz, 1H,), 6.66 (dd, J = 8.8 Hz, 2.4Hz, 1H), 6.49 (d, J = 2.4Hz, 1H), 3.15 (s, 6H); ^{13}C-NMR (CD_3Cl, 100 MHz) δ 187.90, 161.71, 158.57, 155.30, 145.51, 132.20, 114.97, 110.29, 108.50, 97.59, 40.30; HRMS (ESI) calcd for $C_{12}H_{12}NO_3$ $[M+H]^+$ 218.0817, found 218.0820.

.

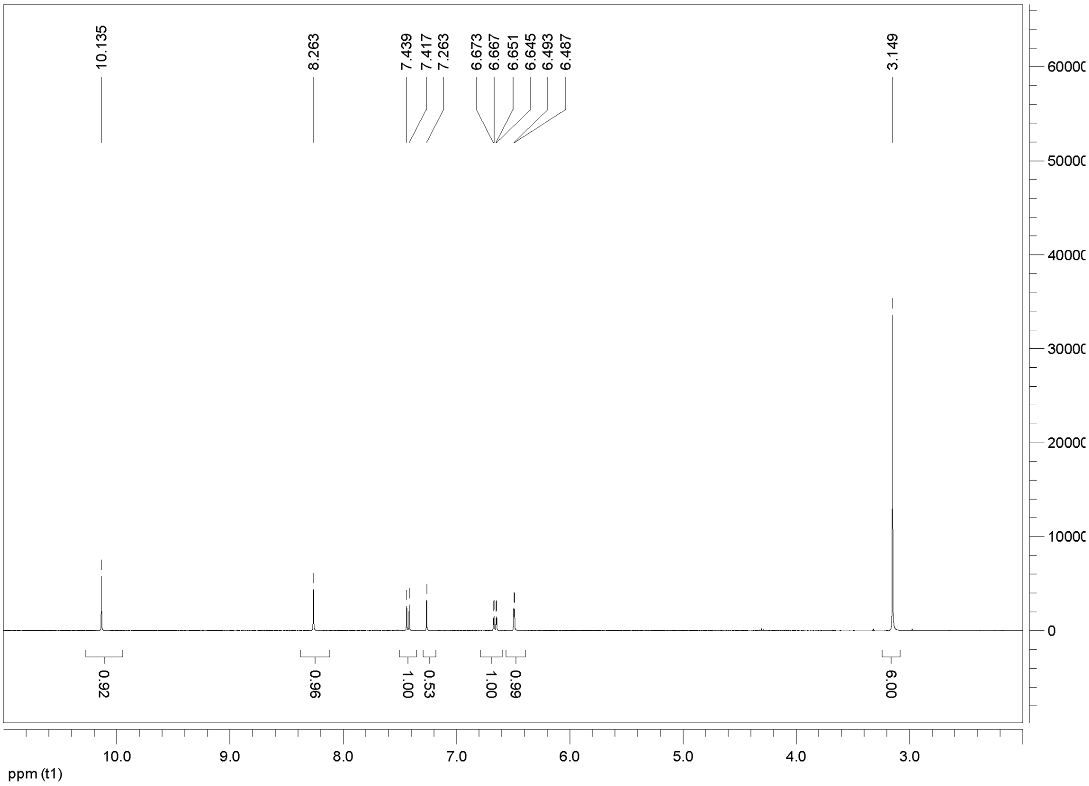

Figure S4: ^{1}H-NMR spectrum of **1** in $CDCl_3$.

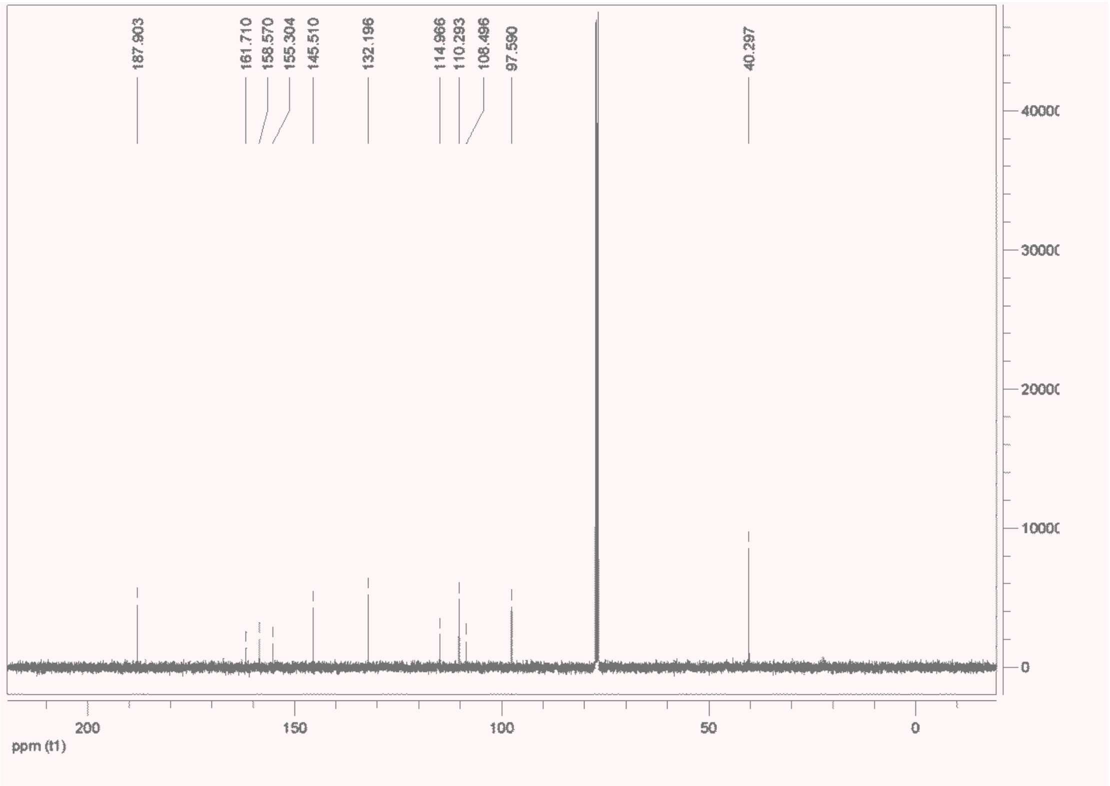

Figure S5: ^{13}C-NMR spectrum of **1** in $CDCl_3$.

Fluorescence Excitation Spectra of 1 in $CHCl_3$

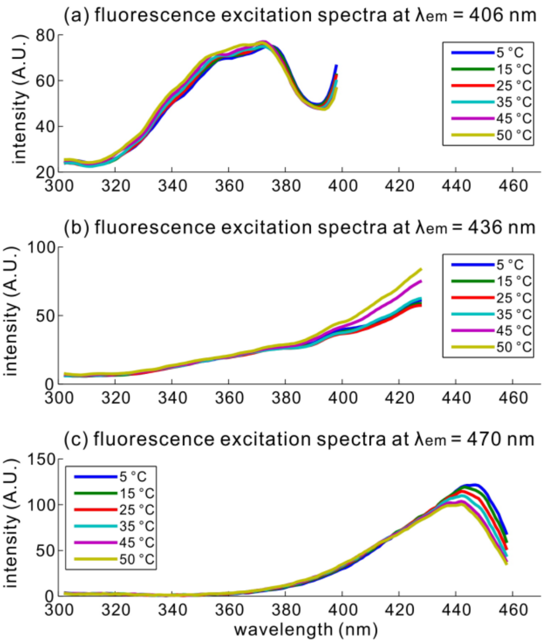

Figure S6: Fluorescence excitation spectra of **1** in $CHCl_3$ ([**1**] = 2 μM).

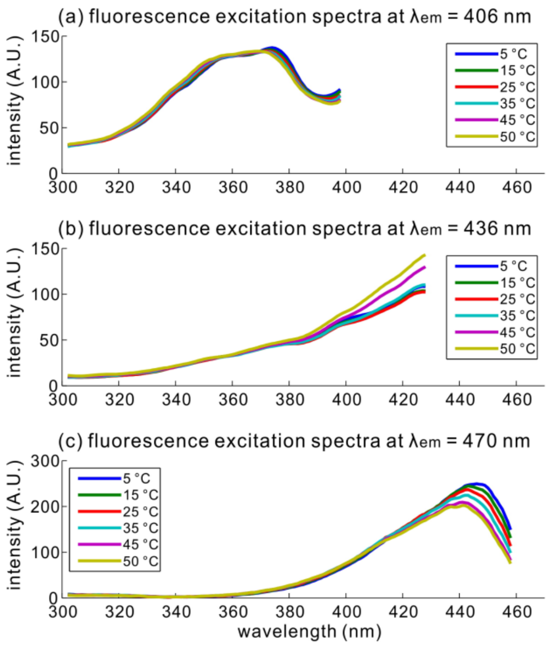

Figure S7: Fluorescence excitation spectra of **1** in $CHCl_3$ ([**1**] = 8 μM).

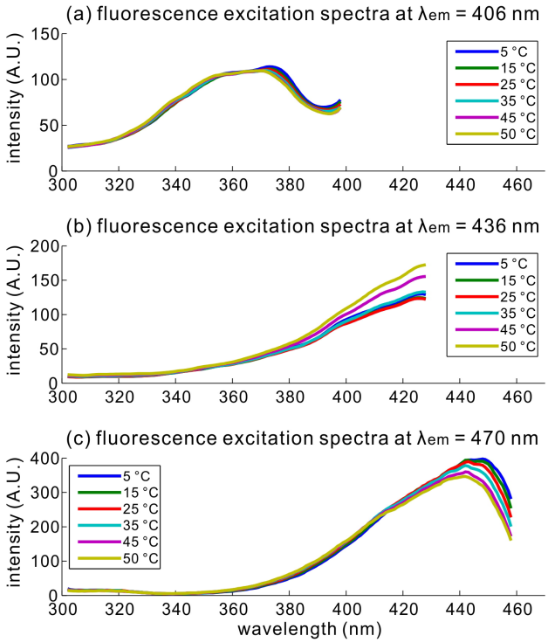

Figure S8: Fluorescence excitation spectra of **1** in $CHCl_3$ ([**1**] = 20 μM).

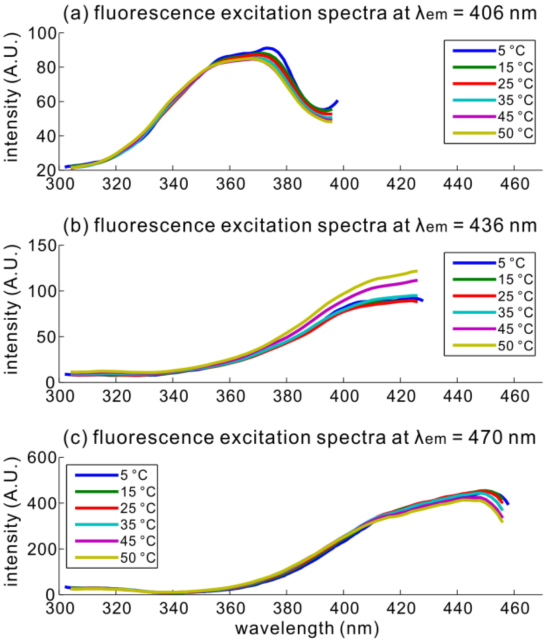

Figure S9: Fluorescence excitation spectra of **1** in $CHCl_3$ ([**1**] = 40 μM).

Concentration Dependence of the ^{1}H-NMR Spectra of 1

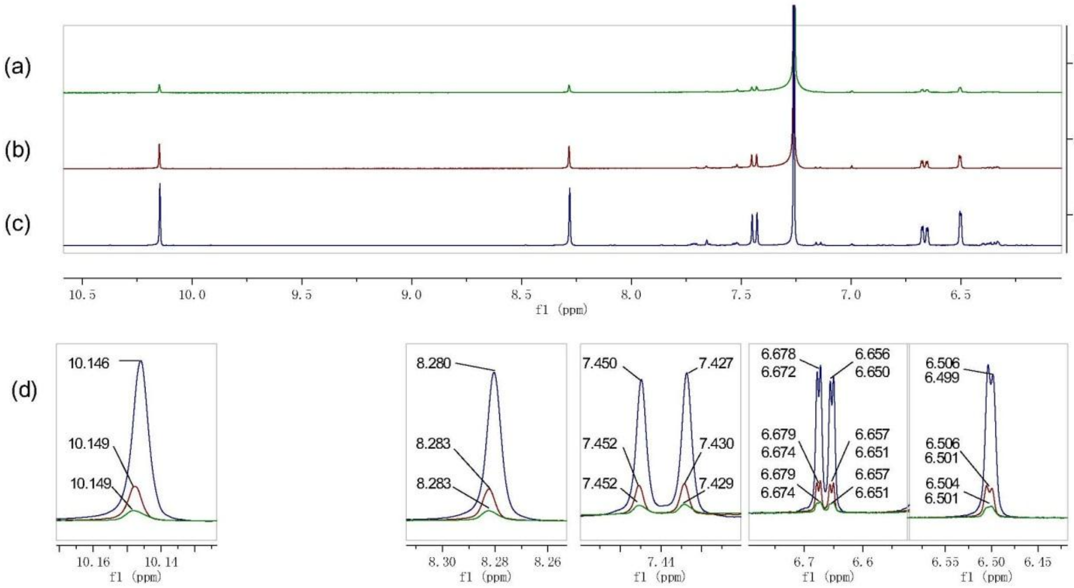

Figure S10: ^{1}H-NMR spectra of **1** in $CDCl_3$ at (a) 0.92 mM; (b) 1.84 mM and (c) 9.2 mM. (d) Superimposed NMR spectra shown in (a)—(c).

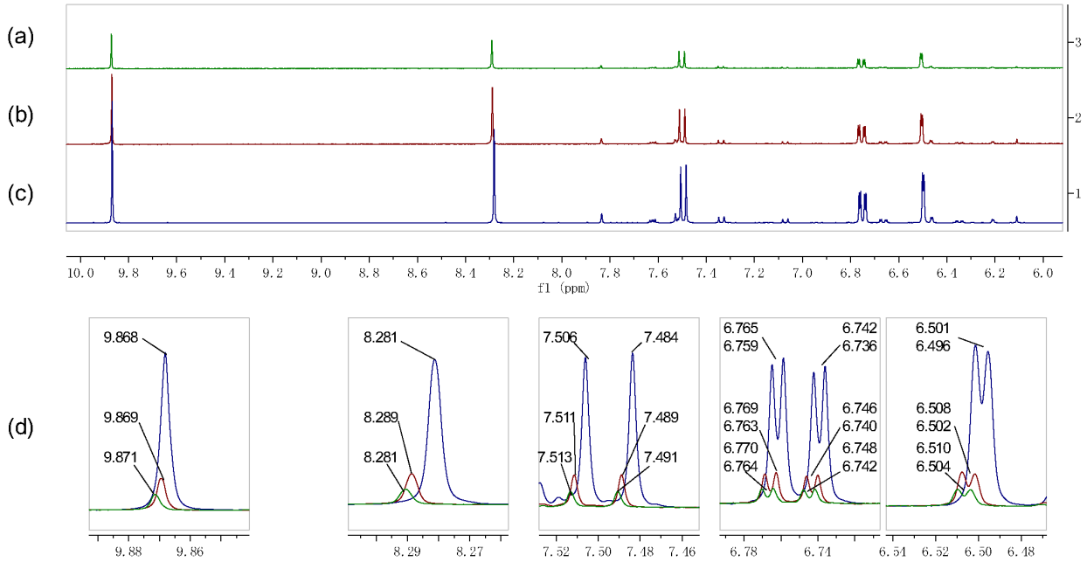

Figure S11: ^{1}H-NMR spectra of **1** in deuterated methanol at (a) 0.92 mM; (b) 1.84 mM and (c) 9.2 mM. (d) Superimposed NMR spectra shown in (a)—(c).

Temperature Dependence of UV-Vis Absorption Spectra of 1 in CHCl$_3$

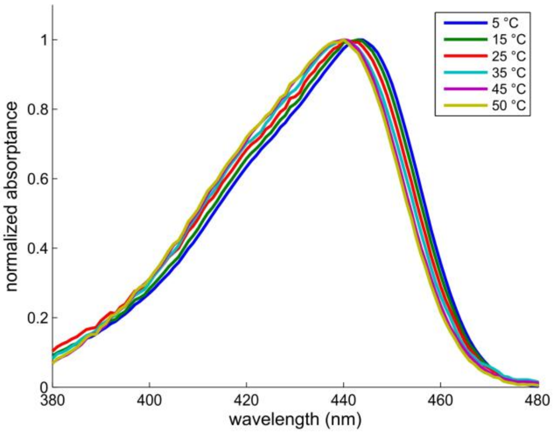

Figure S12: Temperature dependence of the normalized UV-Vis absorption spectra of **1** in CHCl$_3$ ([**1**] = 4 μM).

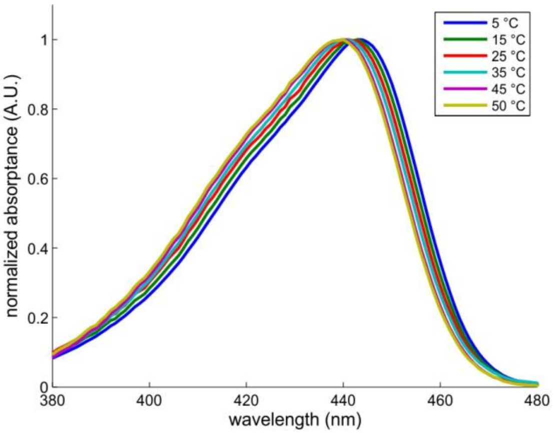

Figure S13: Temperature dependence of the normalized UV-Vis absorption spectra of **1** in $CHCl_3$ ([**1**] = 8 μM).

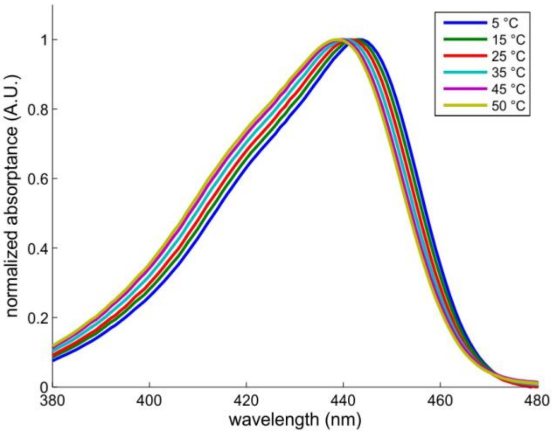

Figure S14: Temperature dependence of the normalized UV-Vis absorption spectra of **1** in $CHCl_3$ ([**1**] = 20 μM).

Summary of Fluorescent Lifetime Measurement Results

Table S1. Summary of Fitting Parameters to the Fluorescence Decay Dynamics of **1**.[a]

λ_{em}	A_1	τ_1	A_2	τ_2	χ^2	$A_1/(A_1+A_2)$	$A_2/(A_1+A_2)$
415 nm	3016.531	1.1 ns	315.136	2.9 ns	1.270	90.5%	9.5%
420 nm	4973.282	1.1 ns	617.171	2.9 ns	1.379	89.0%	11.0%
425 nm	4786.906	1.1 ns	693.501	2.9 ns	1.350	87.3%	12.7%
430 nm	4411.136	1.1 ns	897.392	2.9 ns	1.268	83.1%	16.9%
435 nm	4107.026	1.1 ns	1469.479	2.9 ns	1.374	73.6%	26.4%
440 nm	2946.514	1.1 ns	2314.001	2.9 ns	1.211	56.0%	44.0%
445 nm	1869.814	1.1 ns	3445.265	2.9 ns	1.237	35.2%	64.8%
450 nm	583.662	1.1 ns	2460.699	2.9 ns	1.229	19.2%	80.8%

455 nm	325.342	1.1 ns	2635.605	2.9 ns	1.213	11.0%	89.0%
460 nm	156.401	1.1 ns	2910.295	2.9 ns	1.113	5.1%	94.9%
465 nm	114.239	1.1 ns	2826.581	2.9 ns	1.140	3.9%	96.1%
470 nm	67.504	1.1 ns	3026.141	2.9 ns	1.158	2.2%	97.8%
475 nm	50.926	1.1 ns	2875.73	2.9 ns	1.160	1.7%	98.3%
480 nm	26.802	1.1 ns	3007.302	2.9 ns	1.183	0.9%	99.1%

[a] The fluorescent decay dynamics of **1** can be well modeled by a double-exponential decay function, i.e., $A_1 \exp\left(-\frac{t}{\tau_1}\right) + A_2 \exp\left(-\frac{t}{\tau_2}\right) + B$, owing to both the dimer and monomer emissions. The steady-state contributions of these two emission components are calculated using $\frac{A_1}{A_1+A_2}$ and $\frac{A_2}{A_1+A_2}$, respectively.

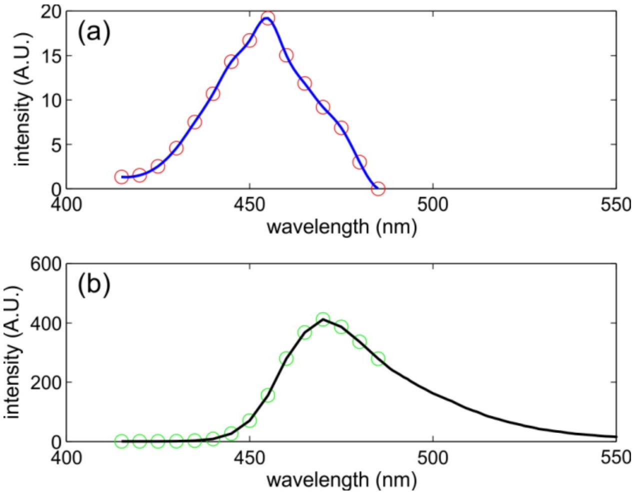

Figure S15: Computed fluorescent spectra of (a) dimers and (b) monomers of **1** in $CHCl_3$ (λ_{ex} = 405 nm, [**1**] = 8 μM).

Temperature Dependence of Emission Intensities of 1

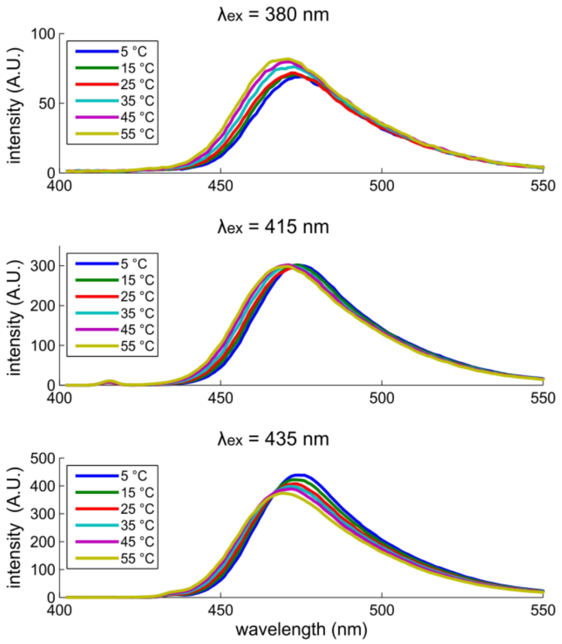

Figure S16: Temperature dependence of fluorescence intensities of **1** in EA ([**1**] = 4 μM) excited at: (a) λ_{ex} = 380 nm; (b) λ_{ex} = 415 nm and (c) λ_{ex} = 435 nm.

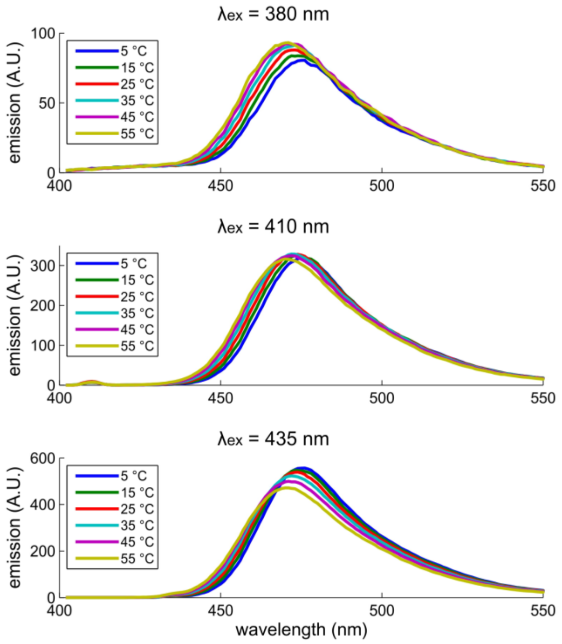

Figure S17: Temperature dependence of fluorescence intensities of **1** in THF ([**1**] = 4 μM) excited at: (a) λ_{ex} = 380 nm; (b) λ_{ex} = 410 nm and (c) λ_{ex} = 435 nm.

Table S2: Temperature Dependence of Fluorescent Intensity Variations of **1** in $CHCl_3$ ([**1**] = 2 μM) from 5 to 50 °C Excited at Various Wavelengths.

excitation wavelength (nm)	max Intensity	min intensity	intensity variation	emission peak shift (nm)
370	7.00	5.37	23.4%	5
375	9.05	7.15	21.0%	6
380	12.35	9.69	21.6%	6
385	16.32	13.00	20.3%	5
390	21.03	17.89	14.9%	8
395	27.32	23.90	12.5%	6
400	35.07	30.99	11.6%	5
405	43.14	39.05	9.5%	4
410	52.63	48.52	7.8%	4
415	**62.08**	**60.58**	**2.4%**	**5**
420	71.18	69.29	2.7%	4
425	82.43	78.31	5.0%	6
430	92.49	87.39	5.5%	5
435	104.73	98.01	6.4%	6
440	116.44	102.13	12.3%	3
445	124.65	94.88	23.9%	7
450	118.93	76.85	35.4%	6

Table S3: Temperature Dependence of Fluorescent Intensity Variations of **1** in $CHCl_3$ ([**1**] = 20 μM) from 5 to 50 °C Excited at Various Wavelengths.

excitation wavelength (nm)	max Intensity	min intensity	intensity variation	emission peak shift (nm)
370	33.85	27.32	19.3%	8
375	45.90	37.27	18.8%	5
380	61.54	50.50	17.9%	4
385	80.68	69.22	14.2%	6
390	102.11	91.25	10.6%	3
395	129.71	119.46	7.9%	5
400	157.88	149.08	5.6%	3
405	191.33	182.19	4.8%	5
410	**224.77**	**218.87**	**2.6%**	**4**
415	258.22	244.98	5.1%	6
420	287.16	264.46	7.9%	4
425	317.05	290.00	8.5%	4
430	342.45	312.22	8.8%	5
435	369.88	336.47	9.0%	5

440	396.06	344.83	12.9%	4
445	412.34	336.26	18.5%	4
450	408.18	298.59	26.8%	5

Table S4: Temperature Dependence of Fluorescent Intensity Variations of **1** in EA ([**1**] = 4 μM) from 5 to 55 °C Excited at Various Wavelengths.

excitation wavelength (nm)	max Intensity	min intensity	intensity variation	emission peak shift (nm)
360	25.34	18.90	25.4%	4
365	35.01	26.72	23.7%	6
370	47.42	38.89	18.0%	5
375	63.26	52.12	17.6%	5
380	81.80	69.10	15.5%	4
385	104.60	90.69	13.3%	5
390	129.85	114.62	11.7%	5
395	164.23	148.24	9.7%	4
400	199.25	185.64	6.8%	5
405	236.42	223.82	5.3%	4
410	270.22	260.70	3.5%	5
415	**302.01**	**294.46**	**2.5%**	**3**
420	339.10	324.37	4.3%	5
425	379.52	359.34	5.3%	5
430	414.14	375.36	9.4%	4
435	438.66	373.90	14.8%	5
440	427.87	335.34	21.6%	4

Table S5: Temperature Dependence of Fluorescent Intensity Variations of **1** in THF ([**1**] = 4 μM) from 5 to 55 °C Excited at Various Wavelengths.

excitation wavelength (nm)	max Intensity	min intensity	intensity variation	emission peak shift (nm)
370	54.65	47.16	13.7%	6
375	71.24	61.20	14.1%	7
380	93.16	80.51	13.6%	5
385	118.65	105.01	11.5%	4
390	149.21	135.40	9.3%	3
395	188.45	172.75	8.3%	5
400	234.46	218.93	6.6%	5
405	281.02	269.44	4.1%	4

410	**328.61**	**316.15**	**3.8%**	**5**
415	376.02	354.42	5.7%	5
420	417.46	389.31	6.7%	4
425	472.41	432.87	8.4%	6
430	518.95	461.71	11.0%	5
435	556.72	471.34	15.3%	6
440	561.95	441.41	21.5%	6
445	525.06	376.48	28.3%	5
450	445.73	291.22	34.7%	6
455	316.76	187.77	40.7%	4
460	191.53	105.06	45.1%	4

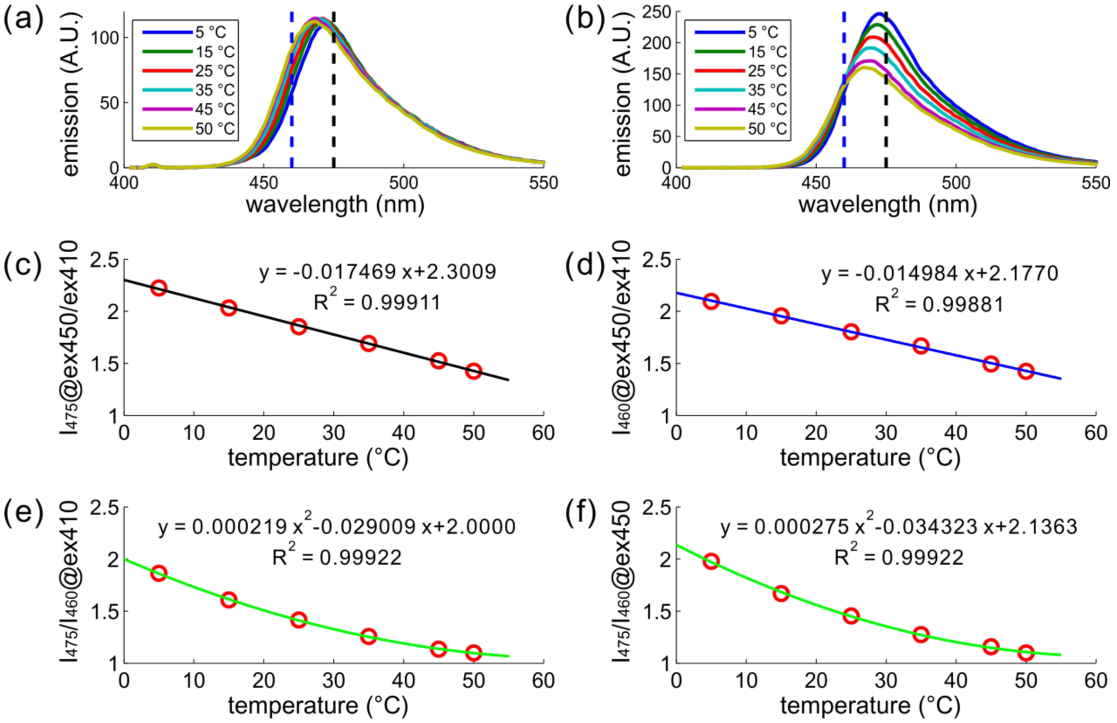

Figure S18: Temperature dependence of fluorescence intensities of **1** excited at (a) 410 nm and (b) 450 nm in $CHCl_3$. Temperature dependence of the ratios of fluorescence intensities and the associated best-fit equations (c) at 475 nm, excited at 450 and 410 nm, respectively; (d) at 460 nm, excited at 450 and 410 nm, respectively; (e) at 475 and 460 nm, excited at 410 nm; (f) at 475 and 460 nm, excited at 450 nm. [**1**] = 8 μM. Two vertical lines at 460 and 475 nm are drawn in (a) and (b), respectively, to illustrate the different temperature dependence of the emission intensities at these two wavelengths.

Note that the temperature calibration curves shown here are slightly different from those in Figure 2 of the main text; these curves are concentration-dependent, since the monomer-aggregation equilibrium depends on the concentration of **1**. However, for a closed system, the concentration of **1** can be precisely controlled, thereof ensuring unique calibration curves.

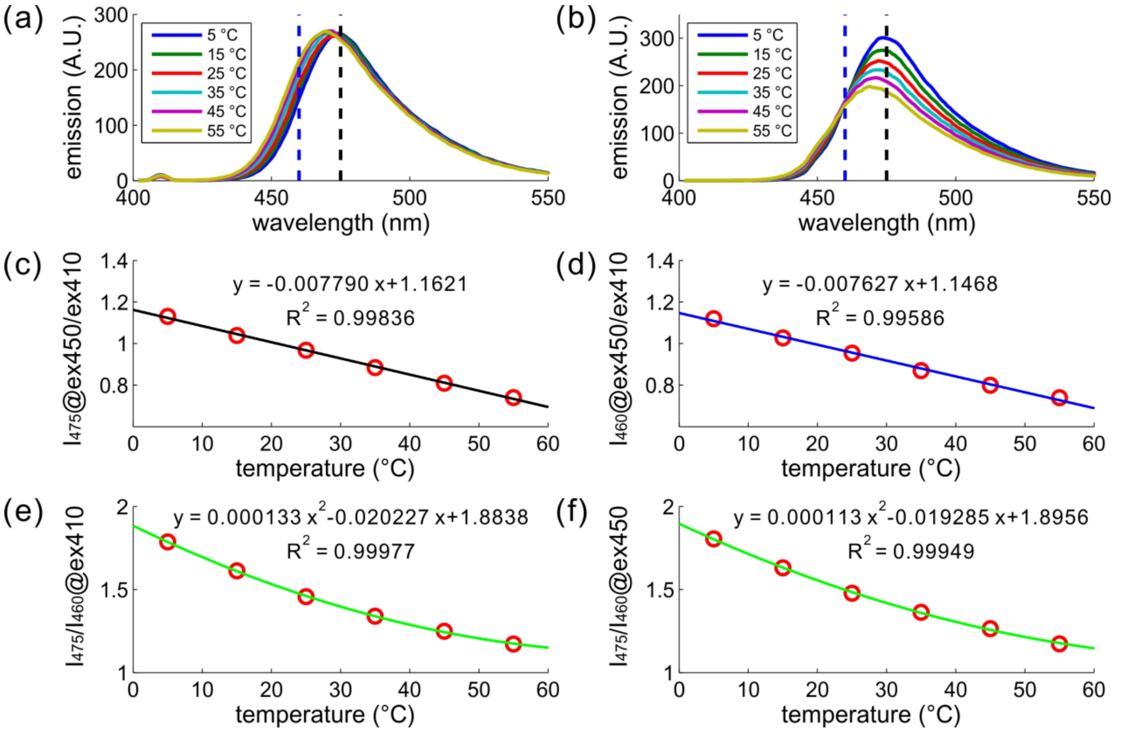

Figure S19: Temperature dependence of fluorescence intensities of **1** excited at (a) 410 nm and (b) 450 nm in EA. Temperature dependence of the ratios of fluorescence intensities and the associated best-fit equations (c) at 475 nm, excited at 450 and 410 nm, respectively; (d) at 460 nm, excited at 450 and 410 nm, respectively; (e) at 475 and 460 nm, excited at 410 nm; (f) at 475 and 460 nm, excited at 450 nm. [**1**] = 4 μM. Two vertical lines at 460 and 475 nm are drawn in (a) and (b), respectively, to illustrate the different temperature dependence of the emission intensities at these two wavelengths.

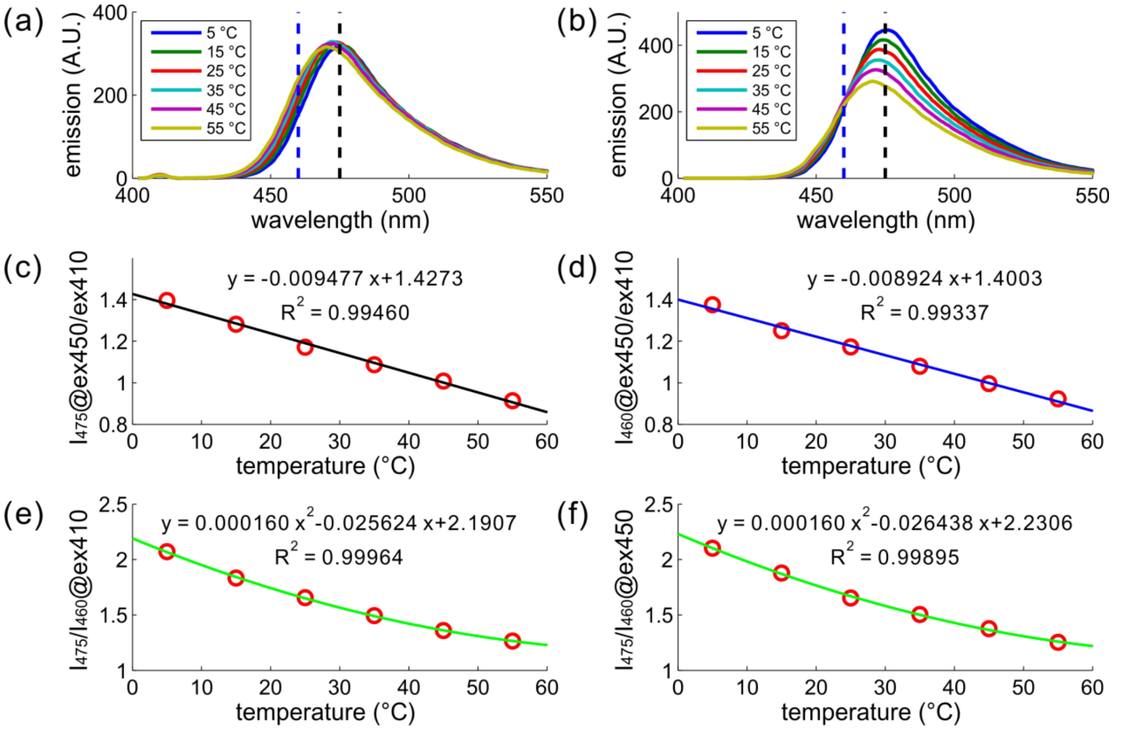

Figure S20: Temperature dependence of fluorescence intensities of **1** excited at (a) 410 nm and (b) 450 nm in THF. Temperature dependence of the ratios of fluorescence intensities and the associated best-fit equations (c) at 475 nm, excited at 450 and 410 nm, respectively; (d) at 460 nm, excited at 450 and 410 nm, respectively; (e) at 475 and 460 nm, excited at 410 nm; (f) at 475 and 460 nm, excited at 450 nm. [**1**] = 4 μM. Two vertical lines at 460 and 475 nm are drawn in (a) and (b), respectively, to illustrate the different temperature dependence of the emission intensities at these two wavelengths.

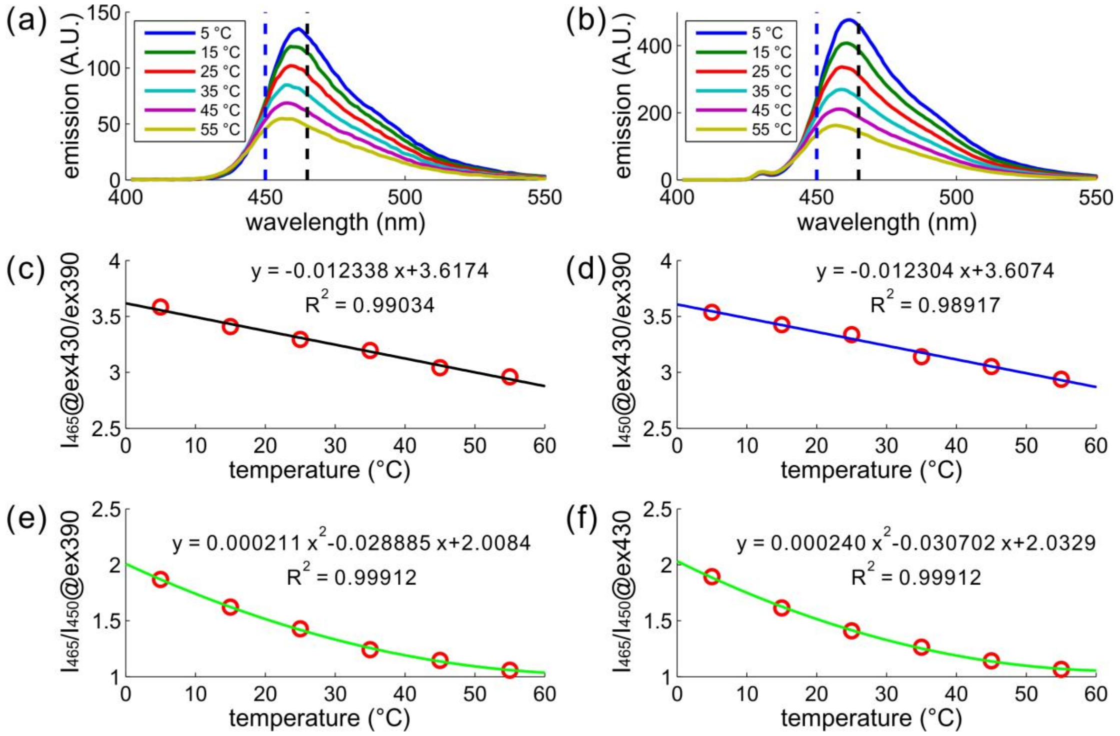

Figure S21: Temperature dependence of fluorescence intensities of **1** excited at (a) 390 nm and (b) 430 nm in toluene. Temperature dependence of the ratios of fluorescence intensities and the associated best-fit equations (c) at 465 nm, excited at 430 and 390 nm, respectively; (d) at 450 nm, excited at 430 and 390 nm, respectively; (e) at 465 and 450 nm, excited at 390 nm; (f) at 465 and 450 nm, excited at 430 nm. [**1**] = 4 μM. Two vertical lines at 450 and 465 nm are drawn in (a) and (b), respectively, to illustrate the different temperature dependence of the emission intensities at these two wavelengths.

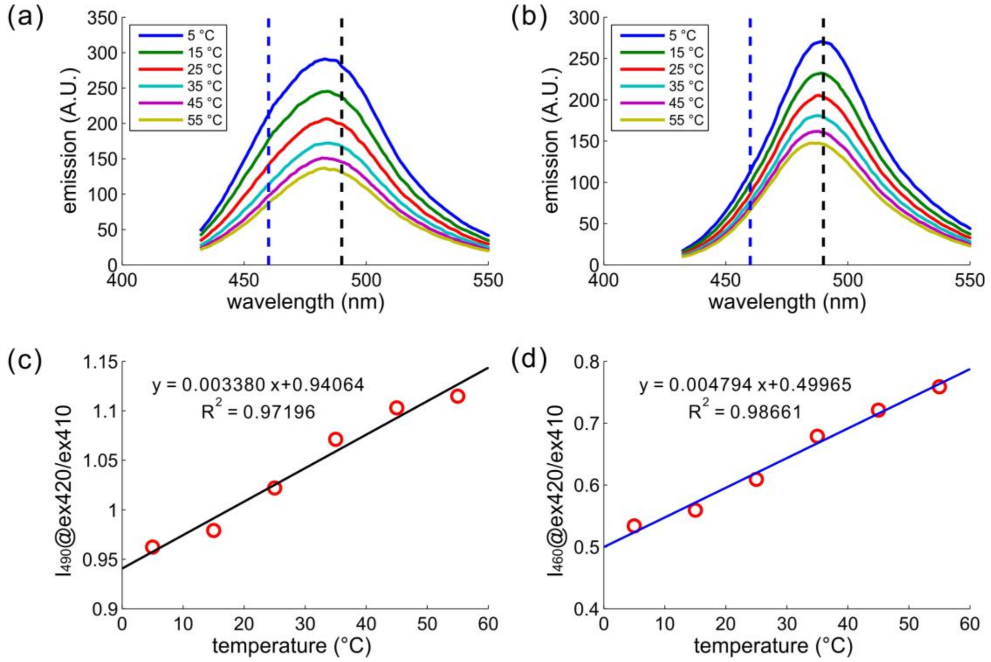

Figure S22: Temperature dependence of fluorescence intensities of **1** excited at (a) 410 nm and (b) 420 nm in methanol. Temperature dependence of the ratios of fluorescence intensities and the associated best-fit equations (c) at 490 nm, excited at 420 and 410 nm, respectively; (d) at 460 nm, excited at 420 and 410 nm, respectively. [**1**] = 4 μM. Two vertical lines at 460 and 490 nm are drawn in (a) and (b), respectively, to illustrate the different temperature dependence of the emission intensities at these two wavelengths.

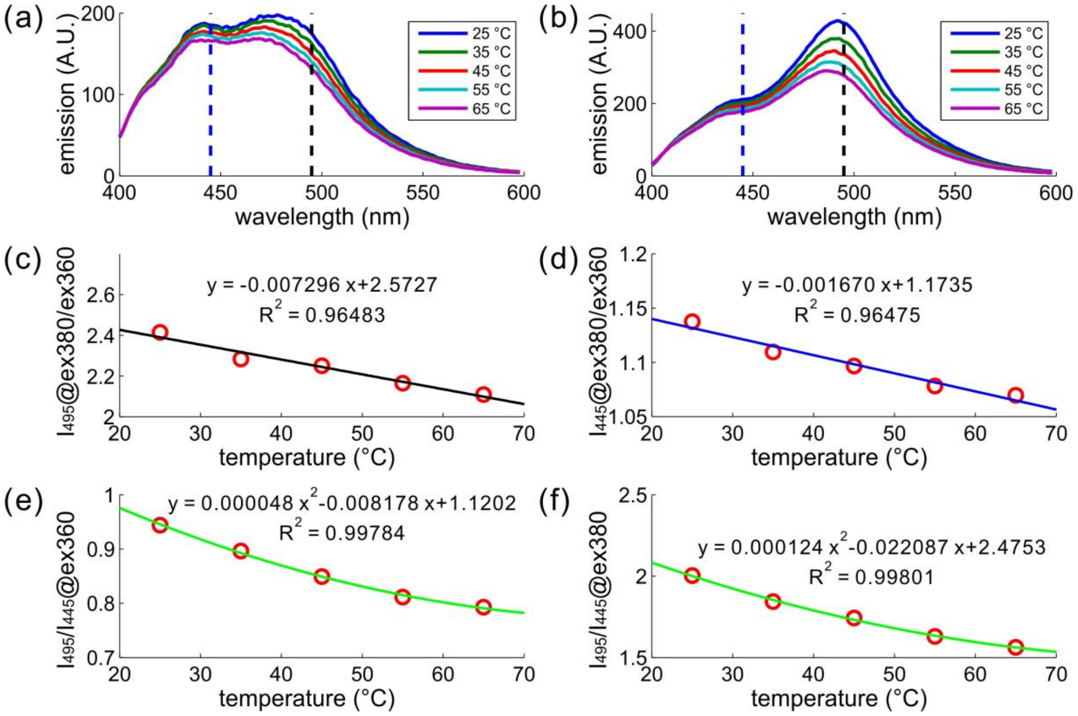

Figure S23: Temperature dependence of fluorescence intensities of **1** excited at (a) 360 nm and (b) 380 nm in DMSO. Temperature dependence of the ratios of fluorescence intensities and the associated best-fit equations (c) at 495 nm, excited at 380 and 360 nm, respectively; (d) at 445 nm, excited at 380 and 360 nm, respectively; (e) at 495 and 445 nm, excited at 360 nm; (f) at 495 and 445 nm, excited at 380 nm. [**1**] = 10 μM. Two vertical lines at 445 and 495 nm are drawn in (a) and (b), respectively, to illustrate the different temperature dependence of the emission intensities at these two wavelengths.

Computational Details

Quantum-chemical calculations were performed on the monomer and dimer of **1** using *Gaussian 09*.[1] Becke's three-parameter and Lee-Yang-Parr hybrid functional (B3LYP)[2-4] and a 6-31+G(d) basis set[5] were used in all calculations.

The geometries of the monomer and dimer of **1** were optimized *in vacuo* and in solution using the polarizable continuum model (PCM) to act as an implicit solvent incorporation.[6,7] $CHCl_3$ solvent was modelled for both the monomer and the dimer, while ethanol and DMSO solvents were modeled only for the monomer. Following this, TD-DFT calculations were carried out on the optimized molecular structures in order to determine their UV-Vis absorption profiles and peak absorption wavelengths (λ_{abs}).

For dimer modelling, D3 version of Grimme's dispersion correction with Becke-Johnson damping (GD3BJ) has been applied in all calculations.[8] The starting dimer structure for the geometry optimization was constructed by modifying the crystal structure of 3-(cyclopropanecarbonyl)-4-hydroxy-2H-chromen-2-one (reference code in Cambridge Structural Database: DESKOC).[9]

In all calculations, frequency checks were performed after each geometry optimization to ensure that minima on the potential energy surfaces were found.

Computational Results

Calculated λ_{abs} values of the monomer of **1** in solvents are smaller than experimental readings (Table S6). In comparison to the experimental absorption peaks of **1** in $CHCl_3$ (centered at ~370, ~395 and ~445 nm), the theoretical value (402.34 nm) is smaller only than the main peak at ~445 nm. Hence, the absorption peak at ~445 nm (or 441 nm as reported by Cigan *et al.*[10]) is assigned to the monomer of **1**, while the other two blue-shifted peaks are attributed to the high-order and low-order H-aggregates of **1**, respectively.

Table S6: Comparison of Theoretical and Experimental λ_{abs} Values of the Monomer of **1** in Neat Solvents.

solvent	theoretical λ_{abs} (nm)	experimental λ_{abs} (nm)[10]
$CHCl_3$	402.34	441
methanol	404.61	436
DMSO	406.76	447

TD-DFT calculations also show that the absorption peaks of dimers appear at shorter wavelengths than those of monomers (Figure S24).

Figure S24: Theoretical UV-Vis absorption spectra of the monomer and dimer of **1** in (a) *vacuo* and (b) $CHCl_3$.

References

1. M. J. Frisch, G. W. Trucks, H. B. Schlegel, G. E. Scuseria, M. A. Robb, J. R. Cheeseman, G. Scalmani, V. Barone, B. Mennucci, G. A. Petersson and et al., Gaussian Inc., Wallingford, CT, 2009.
2. P. J. Stephens, F. J. Devlin, C. F. Chabalowski and M. J. Frisch, *J. Phys. Chem.*, 1994, **98**, 11623-11627.
3. A. D. Becke, *J. Chem. Phys.*, 1993, **98**, 5648-5652.
4. C. Lee, W. Yang and R. G. Parr, *Phys. Rev. B*, 1988, **37**, 785-789.
5. V. A. Rassolov, M. A. Ratner, J. A. Pople, P. C. Redfern and L. A. Curtiss, *J. Comput. Chem.*, 2001, **22**, 976-984.
6. D. M. Chipman, *J. Chem. Phys.*, 2000, **112**, 5558-5565.
7. S. Miertus, E. Scrocco and J. Tomasi, *Chem. Phys.*, 1981, **55**, 117-129.
8. S. Grimme, S. Ehrlich and L. Goerigk, *J. Comput. Chem.*, 2011, **32**, 1456-1465.
9. P.-Y. Kuo, T.-L. Shie, Y.-S. Chen, J.-T. Lai and D.-Y. Yang, *Bioorg. Med. Chem. Lett.*, 2006, **16**, 6024-6027.
10. M. Cigáň, J. Donovalová, V. Szöcs, J. Gašpar, K. Jakusová and A. Gáplovský, *J. Phys. Chem. A*, 2013, **117**, 4870-4883.